Impact of Sequential Ground Motion Pairing on Mainshock-Aftershock Structural Response and Collapse Performance Assessment

Mehrdad Shokrabadi

Henry V. Burton, PhD, PE (PI)

Jonathan P. Stewart. PhD, PE (Co PI)

Department of Civil and Environmental Engineering

University of California, Los Angeles

A report on research conducted under Grant No. G16AP00006 from the U.S. Geological Survey, National Earthquake Hazards Reduction Program.

June 2017

ABSTRACT

USGS Award No G16AP00006

IMPACT OF SEQUENTIAL GROUND MOTION PAIRING ON MAINSHOCK-AFTERSHOCK STRUCTURAL RESPONSE AND COLLAPSE PERFORMANCE ASSESSMENT

PI: Henry V. Burton, Co PI: Jonathan P. Stewart

Department of Civil and Environmental Engineering

University of California, Los Angeles

Los Angeles, CA 90095-1593

Tel: (310) 825-2843 Fax: (310) 206-2222
hvburton@seas.ucla.edu; stewart@seas.ucla.edu

Recent events such as the 2010 Canterbury earthquakes and the 2011 Tohoku earthquake have highlighted the importance of considering both mainshock and aftershock ground motion hazard in the seismic design and performance assessment of buildings. Aftershock events have been shown to exacerbate the damage caused by mainshocks and in some cases have led to collapse. The risk of aftershock collapse also influences the post-mainshock decisions of owners and occupiers regarding re-occupancy of damaged buildings, thereby affecting the recovery process. While the threat posed by aftershocks is now well recognized, research to quantify the associated risk is still in its infancy, particularly with regards to integrating the time-dependent aftershock hazard with the increased vulnerability to collapse of damaged buildings.

Earthquake engineers lack well-founded consensus guidelines for selecting ground motion time series for sequential mainshock-aftershock events for use in seismic performance assessment. Past practice has seen sequences formed by coupling as-recorded mainshock and aftershock records and by using repeated mainshock records for both event types. Using mainshock-mainshock versus mainshock-aftershock record pairs, we assess the structural performance of five ductile reinforced concrete frames with varying heights using sequential nonlinear response history analyses. We find systematic differences in the frequency content of mainshock and aftershock records, which in turn produce expected differences in structural responses conditional on the dynamic characteristics of each structure. The outcome is measurable differences in the structural response, with mainshock-mainshock sequences potentially over- or under-estimating seismic demand and risk relative to the use of more appropriate mainshock-aftershock record pairs. This finding holds true even when mainshock-mainshock sequences are formed by preserving the magnitude and distance relationships between as-recorded mainshocks and aftershocks. The correlation between event terms of mainshock and aftershock ground motions recorded from the same sequence is found to have a significant impact on maximum story drift ratio. We provide recommendations for aftershock record selection that draw upon these results.

ACKNOWLEDGEMENTS

The research presented in this paper is supported by the United States Geological Survey (USGS) EHP Award Number G16AP00006. Any opinions, findings, and conclusions or recommendations expressed in this paper are those of the authors and do not necessarily reflect the views of the sponsor.

TABLE OF CONTENTS

1 INTRODUCTION 9

2 GROUND MOTION SELECTION FOR BUILDING AFTERSHOCK SEISMIC PERFORMANCE ASSESSMENT 13

2.1 Previous studies on the differences in the frequency content of mainshock and aftershock ground motions 13

2.2 Ground Motions used for Mainshock-Aftershock Seismic Performance Assessment 14

2.3 Nonlinear Response Spectra for Ground Motions used for Mainshock-Aftershock Seismic Performance Assessment 18

3 MAINSHOCK-AFTERSHOCK STRUCTURAL RESPONSE AND SEISMIC PERFORMANCE ASSESSMENT 20

3.1 Building Descriptions and Structural Modeling 20

3.2 Impact of correlation between 'parent' and 'children' events in a seismic sequence on SDR 21

3.3 Collapse performance assessment 24

3.3.1 Methodology 24

3.3.2 Outcomes of nonlinear dynamic analyses under the sets of sequential ground motions 28

4 SUMMARY AND CONCLUSION 37

REFERENCES 39

LIST OF FIGURES

FIGURE 2-1. COMPARING THE SPECTRA OF MAINSHOCK AND AFTERSHOCK RECORDS WITH SIMILAR MAGNITUDES OBTAINED FROM THE GMPE BY CHIOU AND YOUNGS [29] 14

FIGURE 2-2. COMPARING A) THE MAGNITUDE VERSUS DISTANCE DISTRIBUTIONS AND B) THE MEDIAN RESPONSE SPECTRA OF THE SECOND-EVENT GROUND MOTIONS IN THE FOUR RECORD-PAIR SETS 17

FIGURE 2-3. COMPARING THE MEDIAN CONSTANT-DUCTILITY RESPONSE SPECTRA FOR THE SECOND GROUND MOTIONS IN THE SS-MS-AS, DS-MS-AS, TG-MS-MS AND MS-MS RECORD SETS FOR SDOFS WITH A) $M = 1$ AND B) $M = 8$ 19

FIGURE 3-1. SCHEMATIC ILLUSTRATION OF THE NUMERICAL MODEL OF THE ARCHETYPES USED FOR NONLINEAR DYNAMIC ANALYSES (AFTER HASELTON ET AL. [43]) 21

FIGURE 3-2. TRENDS BETWEEN MAXIMUM SDR AND DISTANCE FOR THREE DIFFERENT MAGNITUDES AND A) 2-STORY AND B) 20-STORY BUILDINGS 22

FIGURE 3-3. INTRA AND INTER-EVENT RESIDUALS OBTAINED FROM THE TWO-STAGE REGRESSION ANALYSIS ON THE 2- AND 20-STORY BUILDINGS 23

FIGURE 3-4. (A) MAINSHOCK AND B) AFTERSHOCK HAZARD CURVES FOR THE FIVE STUDIED STRUCTURES 27

FIGURE 3-5. COMPARING MEDIAN DRIFT PROFILES UNDER THE UNSCALED SECOND EVENT GROUND MOTIONS IN THE FOUR RECORD-PAIR SETS FOR THE FIVE STUDIED BUILDINGS 30

FIGURE 3-6. COLLAPSE FRAGILITY CURVES FOR THE INTACT AND INCREMENTALLY-INCREASING MAINSHOCK-DAMAGED STATES FOR THE (A) 4- AND (B) 20-STORY STRUCTURES UNDER THE SS-MS-AS SET 31

FIGURE 3-7. COLLAPSE FRAGILITY CURVES OF (A) 2- AND (B) 20-STORY STRUCTURES UNDER THE FOUR RECORD-PAIR SETS IN THE INTACT STATE AFTER THE FIRST EVENT GROUND MOTIONS 32

FIGURE 3-8. RATIO OF (A) LINEAR AND (B) NONLINEAR SPECTRAL ACCELERATIONS OF THE SECOND EVENT GROUND MOTIONS IN THE SS-MS-AS SET TO THE REMAINING THREE SETS 33

FIGURE 3-9. COMPARING P_C FOR AN ASSUMED LIFESPAN OF 50 YEARS FOR A) 2- AND 4-STORY AND B) 8-, 12- AND 20-STORY BUILDINGS UNDER THE SS-MS-AS AND DS-MS-AS SETS OF GROUND MOTIONS 34

FIGURE 3-10. COMPARING P_C FOR AN ASSUMED LIFESPAN OF 50 YEARS FOR A) 2- AND 4-STORY AND B) 8-, 12- AND 20-STORY BUILDINGS UNDER THE SS-MS-AS AND TG-MS-MS SETS OF GROUND MOTIONS 35

FIGURE 3-11. COMPARING PC FOR AN ASSUMED LIFESPAN OF 50 YEARS FOR A) 2- AND 4-STORY AND B) 8-, 12- AND 20-STORY BUILDINGS UNDER THE SS-MS-AS AND MS-MS SETS OF GROUND MOTIONS 36

LIST OF TABLES

TABLE 2-1. EVENT AND RECORD SEQUENCE DEFINITIONS ADOPTED FOR SIMULATIONS CONDUCTED IN THIS STUDY 15

TABLE 2-2. SUMMARY OF P-VALUES FROM KS-TEST ON R, VS30 AND E 17

TABLE 3-1. BASE SHEAR COEFFICIENTS AND PERIODS OF THE FIRST TWO MODES OF EXAMINED BUILDINGS 21

TABLE 3-2 REGRESSION COEFFICIENTS OF EQUATION 1 23

TABLE 3-3. CORRELATION COEFFICIENTS BETWEEN ACTUAL AND RANDOMLY-ASSIGNED 'PARENT' AND MEAN 'CHILDREN' SDR EVENT TERMS 24

TABLE 3-4. LIMIT STATE DESCRIPTION 28

1 INTRODUCTION

The notion of seismic resilience has gained significant attention in earthquake engineering research, education and practice in recent years. Central to achieving seismic resilience is understanding the role that buildings play in ensuring that communities can minimize the effects of, adapt to, and recover from earthquakes [1]. Quantifying the risk of further damage to the built environment from aftershocks is essential to post-mainshock decision-making, functionality and recovery. The compounding effect of the damage and disruption caused by the earthquake sequences in Chi-Chi (1999), Wenchuan (2008), Christchurch (2010-2011), Tohoku (2011) and Central Italy (2016) are just a handful of real-life examples of the human and financial implications of mainshock-aftershock event sequences [2-4].

Advances in nonlinear structural response simulation [5], classifying mainshock-aftershock event sequences (e.g., [6]) and seismic hazard analysis for sequential events (e.g., [7-9]) provide the essential ingredients to characterize structural performance to earthquake sequences. However, prior work on this topic has employed inconsistent protocols for selecting ground motions for event sequences and has not provided the needed insights required to arrive at consensus procedures. We seek to fill this gap in the present study. To help frame the discussion, it is useful at this stage to identify four approaches, most of which have been considered in various forms in the literature:

1. MS-MS (mainshock-mainshock): Select ground motions for both events in the sequence from earthquakes classified as mainshocks [10-15]. The second ground motion in an MS-MS sequence can be a scaled or an unscaled version of the first or a different motion selected from a database of mainshock recordings. As used here, the second recording in an MS-MS sequence is not selected to represent the different source and path attributes of mainshocks and aftershocks.
2. TG-MS-MS (targeted mainshock-mainshock): The second ground motion in the pair, while recorded from a mainshock event, is selected to (as best as possible) match the characteristics of an aftershock motion i.e. lower magnitude and larger rupture distance than the first ground motion.
3. SS-MS-AS (same-sequence mainshock-aftershock): First and second event records taken from recordings of mainshock and aftershocks from the same sequence (e.g., Northridge earthquake mainshock and Northridge aftershocks). Most of the previous studies that

utilized mainshock-aftershock ground motions were done with SS-MS-AS record-pairs [16-18].

4. DS-MS-AS (different-sequence mainshock-aftershock): Same as SS-MS-AS, but the first and second event records are now taken from two different sequences.

Several considerations affect the characteristics of aftershock ground motions, conditional upon the occurrence of a mainshock. First are implications for source and path − aftershocks are generally smaller in magnitude [19] and, for the same site, have larger source-to-site distances (as a result of having smaller rupture area compared to mainshocks) than their parent mainshocks. Second, even when source and path differences are accounted for, evidence has been found of mild correlation between attributes of mainshock and aftershock records belonging to the same sequence [20]. SS-MS-AS record pairs can be considered "ideal" for sequential response history analysis because they would naturally capture these relationships between mainshock and aftershock ground motions. However, allowing for other constraints affecting ground motion selection for nonlinear response history analyses (e.g. matching target $\mathbf{M}$, R, V_{s30}, directivity conditions, and ε from hazard deaggregation), it may not be possible to adequately populate an SS-MS-AS record set. Using DS-MS-AS record-pairs would allow access to a broader pool of ground motions, which has obvious benefits, but at the cost of likely not preserving within-sequence ground motion correlations (as noted by Boore et al. [20]).

A few studies have investigated differences in the dynamic response of structures subjected to MS-MS and MS-AS sequences. Goda [16] compared the ductility demands imposed by MS-MS and SS-MS-AS sequences. The MS-MS sequences were selected such that the distribution of the magnitude of the event producing the second motion in the pair would match the aftershock magnitude distribution predicted by Omori's law [21]. As such, the MS-MS sequence used by Goda [13] could be considered as TG-MS-MS, although the effects of different rupture distances were not considered. A third foreshock-MS-MS sequence was also considered (originally proposed by Hatzigeorgiou and Beskos [10]) in which foreshock and aftershock records are scaled versions of mainshock records (factor of 0.85). The probability distribution of the peak ductility demands developed for a set of single-degree-of-freedom (SDOF) structures with different periods showed slight differences between responses obtained from the SS-MS-AS record-pairs and the MS-MS sequences generated based on Omori's law. The triad sequence produced significantly higher peak ductility demands. In a separate study, Goda [22] compared

the collapse performance of a 2-story wood-frame building under both MS-MS and SS-MS-AS ground motion pairs. Unlike in Goda [13], in this case the MS-MS sequence used the same records in the second event as in the first. Not surprisingly, the MS-MS sequence produced higher collapse probabilities than SS-MS-AS. Ruiz-García [17] conducted a similar study using two low- and mid-height steel frames and reached the same conclusion.

From these prior studies, it is clear that MS-MS sequences are more damaging to structures than MS-AS sequences in which ground motions for the second event more accurately capture attributes of aftershock ground motions. However, there are several gaps in the state of knowledge pertaining to mainshock-aftershock record selection that we seek to address here, specifically:

1. *Is the correlation of ground motions from parent mainshocks to children aftershocks significant with respect to seismic response demands in structures?* We investigate this using carefully selected SS-MS-AS and DS-MS-AS record sequences.
2. *With suitable consideration of source and path differences between mainshocks and aftershocks, can records be selected from mainshock databases to represent the effects of aftershocks?* We investigate this by comparing responses obtained using TG-MS-MS sequences with those from SS-MS-AS.

Two other attributes of our study are distinct from prior work and are significant with respect to the aim of answering the above questions. First, whereas prior work has considered SDOF or multi-degree-of-freedom (MDOF) structures within a small period range, we use five realistic structural models of reinforced concrete frame structures ranging in height from 2- to 20-stories. The multi-mode responses inherent to such models, over a wide period range, is important to assess the impact of alternate record selection protocols.

A second important attribute, elaborated upon in Section 2.2, is that we select ground motions for the alternate suites such that the characteristics that are likely to impact the results of response history analyses (e.g., ε and V_{s30}) are similar. This control on record selection has not been exercised in prior studies [13, 14, 19]. This in an important feature of the selected record-pair sets that would ensure that the differences observed in the structural response under the four record-pair sets stem from the approach used to form the sequences and not the ground motion characteristics that can be controlled for when selecting the record-pairs.

Drawing upon the lessons from prior work, and the insights gained by resolving the above questions, we provide recommendations for selecting record-pairs for use in sequential response history analysis. We seek to accurately represent attributes of realistic ground motion sequences with due consideration of the constraints of record availability from the two event types. Lastly, we demonstrate the collapse safety of the five studied RC buildings using risk-based metrics, which also consider the effect of time-dependent aftershock hazard.

2 GROUND MOTION SELECTION FOR BUILDING AFTERSHOCK SEISMIC PERFORMANCE ASSESSMENT

2.1 Previous studies on the differences in the frequency content of mainshock and aftershock ground motions

An important question that arises when selecting record-pairs for aftershock seismic performance assessment is whether it is appropriate to use mainshock-mainshock (MS-MS or TG-MS-MS) sequences for response history analyses. Previous studies have demonstrated that the response demand on a structure is significantly affected by the frequency content of the ground motion that is used in the analysis [23-25]. As such, any systematic differences in the frequency content of mainshock and aftershock records that are present after controlling for other characteristics (e.g. **M**, R, V_{s30} and ε) would bias the results of aftershock performance assessments conducted using MS-MS or TG-MS-MS ground motions. On the other hand, if no significant differences are found, there is no need to be confined to the relatively limited library of the aftershock ground motions in selecting record-pairs. This section highlights previous studies related to this question.

Although based on a limited dataset, Boore and Atkinson [26] reported a difference in the magnitude scaling of spectral values of the mainshock and aftershock records from the 1985-1988 Nahanni and Miramichi earthquakes. In a different approach, Ruiz-García and Negrete-Manriquez [18] examined the predominant period (T_g) and bandwidth (Ω) of mainshock and aftershock ground motions recorded from seismic events in California. T_g is the period at which the maximum pseudo spectral velocity of a 5%-damped SDOF occurs and Ω is a measure of how the spectral amplitudes of a ground motion are scattered around its central period. Ruiz-Garcia and Negrete-Manriquez reported a wider Ω for aftershock records and a weak correlation between the T_g of the mainshocks and aftershocks.

The difference in the frequency content of mainshock and aftershock ground motions has also been the subject of debate, specifically as it relates to the development of recent ground motion models (GMMs). Using a systematic approach to compare ground motions that allows for controlling the source and site characteristics (e.g. **M**, R), Boore et al. [20] examined the correlation of event terms from parent mainshocks and their children aftershock using the PEER NGA-West 2 database [27]. A mild correlation between the event terms was observed. No

adjustment for aftershocks was included in the final functional form of their GMM as the difference between the event terms of mainshocks and average of event terms from aftershocks was practically zero and independent of magnitude.

For the original NGA project [25], functional forms used in some of the GMMs included a term to distinguish mainshocks from aftershocks. Abrahamson et al. [28] found that the median of spectral values of aftershocks at short periods are smaller than those from similar mainshocks, whereas at longer periods (> 0.75 sec) the aftershock spectral ordinates were larger. As shown in Figure 2-1, Chiou and Youngs [29] reached a similar conclusion, but the transition from lower to higher spectral ordinates (of aftershocks relative to mainshocks) was about 2.0 sec. Such a relationship between S_a values of mainshocks and aftershocks needs to be viewed in the context of the different **M** and *R* expected for these two event types. Whereas aftershock demands will generally be smaller (due to lower **M** and larger *R*), their spectral shape is different from that of mainshocks as shown in Figure 2-1. Chiou and Youngs also found that for aftershocks, the style of faulting had a smaller influence on the predicted spectral values, when compared to mainshocks. On the other hand, the depth to top of rupture (Z_{TOR}) had a stronger influence on the predictions made for aftershocks.

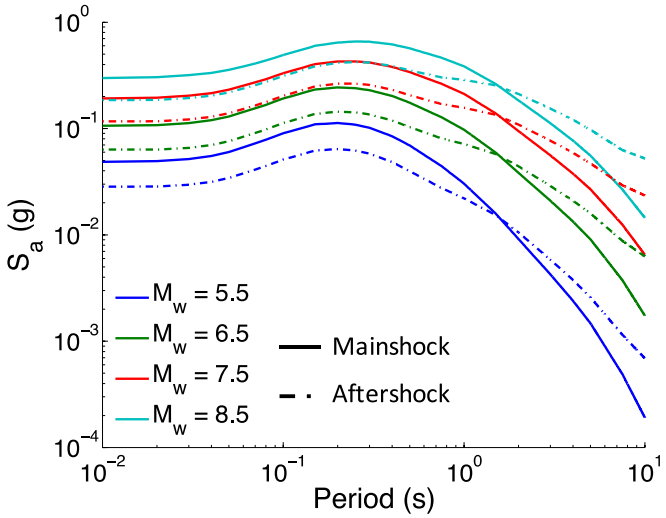

Figure 2-1. Comparing the spectra of mainshock and aftershock records with similar magnitudes obtained from the GMPE by Chiou and Youngs [29]

2.2 Ground Motions used for Mainshock-Aftershock Seismic Performance Assessment

Four sets of sequential ground motions are used for the seismic performance assessment. Each set contains 25 record-pairs selected from the PEER NGA-West2, K-NET and KiK-net

databases. The first ground motion in each record-pair is from an event classified as a 'mainshock' in both databases whereas the second ground motion could be recorded from either a 'mainshock' or 'aftershock' event. Table 2-1 describes the selection of records for the two events in the sequence with respect to the attributes of the second event and attributes of the selected ground motion. The mainshock-aftershock classification for the ground motions selected from the PEER NGA-West2 database is based on the time and distance windowing algorithms developed by Wooddell and Abrahamson [3] while the classification for the K-NET and KiK-net databases is adopted from Goda [16], with a distance window based on Kagan [30] and a time window of 90 days.

Table 2-1. Event and record sequence definitions adopted for simulations conducted in this study

Sequence notation	2nd (aftershock) event attribute	2nd event record attributes[1]
MS-MS: Mainshock-mainshock	Matches MS	Matches MS record
DS-MS-AS: MS and AS records from different event sequences	Distinct: -1.0 **M** unit (average), larger in *R*	Selected from AS record database, any event sequence
TG-MS-MS: Targeted MS-MS sequence	Distinct: -1.0 **M** unit (average), larger in *R*	Selected from MS record database
SS-MS-AS: MS and AS records from same event sequence	Distinct: **M** and *R* per natural sequence attributes	Selected from AS records following MS event in sequence

[1] in all cases, records from first event taken from mainshock records database

For the MS-MS set, the second ground motion in the sequence is the same as the first. This set is included because it represents a common approach in the literature.

The second ground motions in the DS-MS-AS sequences are recorded from aftershock events. However, the mainshock and aftershock ground motion in each pair do not necessarily belong to the same event sequence. Given that aftershocks are generally smaller in magnitude than their preceding mainshocks [19], the aftershocks in this set are selected such that they are on average 1 magnitude unit smaller than the mainshocks. This assumed value is the average of the difference between the magnitudes of mainshock and aftershock events in a database of approximately 2800 records that was used to select the ground motions used for nonlinear dynamic analysis. While there are no specific rules governing the relative source-to-site distance for mainshocks and aftershocks, for the DS-MS-AS set, the second ground motions in the

sequences are selected to have a larger source-to-site distance than the first. The effect of 'parent' and 'children' correlation on aftershock collapse risk is evaluated by comparing the results from the DS-MS-AS and SS-MS-AS record-pair sets. An evaluation of the effect of parent-children on story drift ratio demands is also presented in Section 3.2.

The set of 25 TG-MS-MS record-pairs consists of two mainshock ground motions. The second ground motion is from mainshock events that are on average 1.0 magnitude unit smaller and at the same time larger in distance than those of the first. Comparing the results from the SS-MS-AS and TG-MS-MS record-pair sets informs whether using mainshock ground motions as both records biases computed EDPs. If these two sets yield comparable results, the more comprehensive databases of mainshock ground motions can be used to assemble record-pairs, provided that an appropriate mainshock-aftershock magnitude and distance relationship is applied.

The SS-MS-AS set takes aftershock ground motions from the same event sequence as the mainshock. As such, this is the option in Table 2-1 that most reliably conforms to reality, and is the benchmark against which the two other schemes can be compared.

All record-pairs were selected such that the empirical probabilistic distributions of R, V_{s30} and ε values of the second-event ground motions are similar across the four sets. As discussed before, this ensures that observed differences in seismic response are not due to differences in these ground motion characteristics. The empirical cumulative distribution functions (CDF) of R, V_{s30} and ε for the second-event ground motion in the four record-pair-sets are compared using the two-sample Kolmogorov-Smirnov (KS) test [31]. A statistical hypothesis test is performed where the null hypothesis is that the R, V_{s30} and ε values in any two sets follow the same empirical CDF. The output of the tests is expressed in the form of a $p-value$, which corresponds to the probability that the R, V_{s30} and ε values for two suites of ground motions are from identical probabilistic distributions. A $p-value$ of 5% is used as the acceptable margin [25]. If the $p-value$ obtained from the hypothesis test falls below 5%, then the difference between the R, V_{s30} and ε values of the records is deemed significant. A summary of the results from the KS-tests is shown in Table 2-2. As illustrated, almost all $p-values$ among the four sets of record-pairs are greater than 5%, confirming similarity in the distributions of R, V_{s30} and ε.

Table 2-2. Summary of $\boldsymbol{p-values}$ from KS-Test on $\boldsymbol{R}$, $\boldsymbol{V_{s30}}$ and $\boldsymbol{\varepsilon}$

Record-Pair Sets	r-Values from KS-Test											
	SS-MS-AS			DS-MS-AS			TG-MS-MS			MS-MS		
	V_{s30}	R	ε	V_{s30}	R	ε	V_{s30}	R	ε	V_{s30}	R	ε
SS-MS-AS	1.00	1.00	1.00	0.88	0.99	0.41	0.41	0.24	0.41	0.88	0.06	0.12
DS-MS-AS				1.00	1.00	1.00	0.03	0.12	0.65	0.12	0.06	0.24
TG-MS-MS							1.00	1.00	1.00	1.00	0.24	0.88
MS-MS										1.00	1.00	1.00

Figure 2-2a compares the magnitude versus distance distributions for the second-event ground motion in the four record-pair sets used for response history analysis. The upper and lower bounds on **M** is 5.6 and 7.6 respectively. The median spectra of the second-event ground motion in the record-pair-sets are compared in Figure 2-2b. The spectral values of the second-event ground motion in the TG-MS-MS set are generally higher than the aftershock ground motion in the SS-MS-AS sets up to a period of about 2.0s, beyond which the spectral values of aftershock records approach or exceed those of the mainshocks. This observation is consistent with the trend predicted by the Chiou and Young GMPE [29]. This is an interesting observation given that **M** for the TG-MS-MS records are generally higher than those of the SS-MS-AS set.

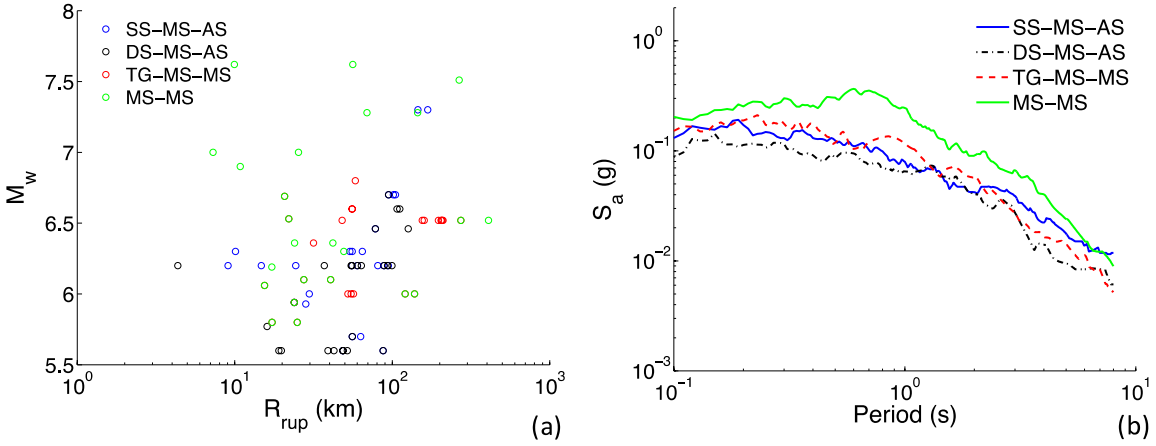

Figure 2-2. Comparing a) the magnitude versus distance distributions and b) the median response spectra of the second-event ground motions in the four record-pair sets

As noted previously, one of the objectives of this work is to investigate the impact of mainshock-aftershock ground motion correlations on structural response EDPs. This is facilitated

by the SS-MS-AS sequence, which implicitly contains these correlations, whereas others do not. To investigate the impact of SS-MS-AS correlation on EDPs, we develop subsequently (Section 3.2) a prediction equation for maximum story drift ratio (SDR). By examining event-specific residuals relative to this prediction equation, we examine the impact of the correlation between parent and children events [20] on SDR values for the five RC buildings.

To support development of the EDP prediction equation, we utilize SDR values obtained using a separate set of ground motions from those used in the sequence analyses (Table 2-1). For this application, we selected 620 ground motions from the NGA-West2 database, recorded from 17 parent mainshock events and their associated 27 children aftershocks as well as a set of 474 mainshock-mainshock ground motions. All of the records have **M** > 4.5 and R_{jb} < 100 km. The methodology used to interpret EDPs derived from these time series is presented in Section 3.2.

2.3 Nonlinear Response Spectra for Ground Motions used for Mainshock-Aftershock Seismic Performance Assessment

A linear response spectrum provides insight into the frequency content of a ground motion. However, it is well known that the displacement demand in a nonlinear SDOF could be significantly larger than that of a linear SDOF when subjected to the same ground motions [32-35]. Past studies on the dynamic response of SDOFs have shown that the ratio of maximum displacements in nonlinear and linear SDOFs (C_u) can significantly exceed unity at short periods and for highly ductile systems [33-36]. Moreover, the response of nonlinear SDOFs are more representative of the behavior of nonlinear MDOF structures. In light of this, constant-ductility inelastic response spectra [37] of elastic-perfectly plastic (EPP) SDOFs, shown in Figure 2-3, are used to compare the response demands from the second ground motion in the SS-MS-AS, TG-MS-MS and MS-MS record-pairs. The ductility factor (μ) is defined as the ratio of the maximum displacement in the EPP SDOF to its yield displacement from response history analysis. The nonlinear pseudo acceleration (A_y) is defined as $A_y = \omega_n^2 u_y$ [37], where u_y is the yield displacement of the nonlinear SDOF.

The normalized A_y spectra in Figure 2-3 suggest that as μ increases, the point at which the spectral values of the aftershock ground motions exceed those of the mainshocks shifts towards lower periods. If the equal displacement rule holds, a higher ductility factor means that yielding in the SDOF happens at lower intensities. Consequently, because of period elongation, such a

system would be more sensitive to the low-frequency contents of the records where, conditioned on similar $\mathbf{M}, R, V_{s30}$ and ε, the spectral demand in aftershock ground motions are expected to be higher than those of mainshock records. This implies that structural systems with higher levels of ductility (as it is the case with most modern code-conforming frame structures) and moderate to long periods are more likely to undergo higher seismic demands when subjected to aftershock ground motions compared to mainshock records. The constant-ductility median response spectra of the second records in the SS-MS-AS and MS-MS sets are also compared in Figure 2-3. Even though the second-event ground motions in the SS-MS-AS set are on average 0.4 **M** smaller than those in the MS-MS set, the median A_y values from the former approach the latter at periods above approximately 2 seconds. In Section 3.3.2 we will examine the implications of these observed differences in the characteristics of mainshock and aftershock ground motions on the seismic performance of the five RC frame buildings.

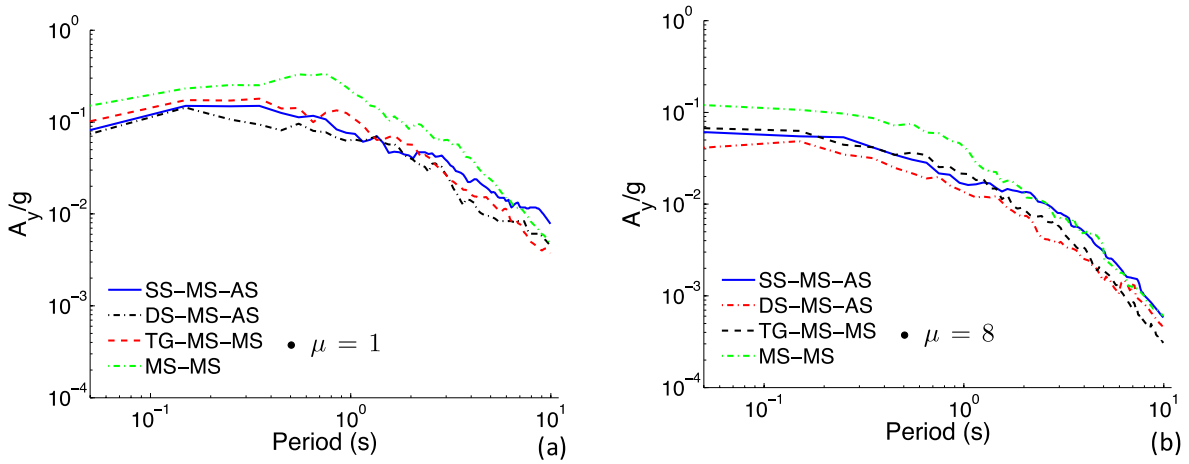

Figure 2-3. Comparing the median constant-ductility response spectra for the second ground motions in the SS-MS-AS, DS-MS-AS, TG-MS-MS and MS-MS record sets for SDOFs with a) $\boldsymbol{\mu = 1}$ and b) $\boldsymbol{\mu = 8}$

3 MAINSHOCK-AFTERSHOCK STRUCTURAL RESPONSE AND SEISMIC PERFORMANCE ASSESSMENT

The mainshock-aftershock structural response and seismic performance of a set of RC moment frames is assessed in this section. The goal is to quantify the effects of different record-pairs on story drift demands, collapse risk and vulnerability.

3.1 Building Descriptions and Structural Modeling

Five modern, code-conforming RC moment-resisting frame buildings are used for this study. The buildings and structural models, adopted from Haselton [38], include 2-, 4-, 8-, 12- and 20-story RC moment frames designed based on the provisions of ASCE 7-05 [39] and ACI 318-02 [40] for a high seismicity site in Los Angeles. The buildings were chosen to incorporate a broad period-range to evaluate whether the effects of alternate record-pairs varies across structure periods. The seismic response of the 2-story, and to a lesser extent the 4-story, structure is mostly influenced by the high frequency energy of ground motions due to their low first-mode period (T_1). A broader range of frequencies influence the response of taller buildings because of their high T_1 and the presence of significant higher-mode effects. 2-D numerical models of the buildings developed by Haselton [38] in the OpenSees platform [41] are utilized for the nonlinear dynamic analyses. Each model consists of three bays of moment-resisting RC frames. The destabilizing effect of the tributary loads on the gravity frames are included through a $P-\Delta$ column. The beams and columns are modeled as elastic elements with nonlinear flexural hinges that incorporate a trilinear backbone curve and hysteretic rules developed by Ibarra et al. [42]. Figure 3-1 shows a schematic layout of the numerical model. Table 3-1 summarizes the design information as well as the periods of the first two modes of each building.

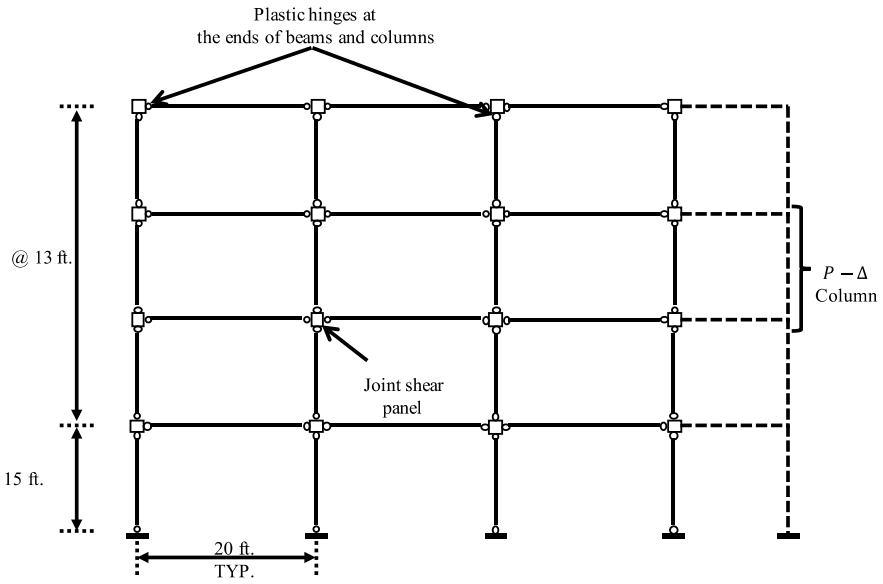

Figure 3-1. Schematic illustration of the numerical model of the archetypes used for nonlinear dynamic analyses (after Haselton et al. [43])

Table 3-1. Base shear coefficients and periods of the first two modes of examined buildings

Building ID[a]	Number of stories	C_s [b]	$C_{s,y}$ [c]	Period (seconds)	
				1st mode	2nd mode
2064	2	0.125	0.392	0.66	0.18
1003	4	0.092	0.143	1.12	0.33
1011	8	0.050	0.077	1.71	0.57
1013	12	0.044	0.075	2.01	0.68
1020	20	0.044	0.070	2.63	0.85

[a] From Haselton [38]

[b] Design base shear coefficient

[c] Yield base shear coefficient

3.2 Impact of correlation between 'parent' and 'children' events in a seismic sequence on SDR

In this section, we examine the possible impact of correlation between ground motions from parent mainshock events and their and children aftershock events. Correlation effects have been observed previously on ground motion intensity measures [20]; the present focus is on the maximum SDR of the RC moment frame structures subjected to ground motions from those event sequences.

Section 2.2 described record selection for this investigation, which produced 620 recordings from 17 parent mainshocks and 27 children aftershocks and a separate set with 474 only-

mainshock ground motions from 18 events. SDR is computed for each nonlinear response history analysis using the five structure models. For a given structural model, we relate the natural log of SDR to the independent variables of moment magnitude (**M**), closest distance to surface projection of fault (R_{JB}), site parameter (V_{S30}) and dummy variables related to fault type (1 for strike slip, 2 for normal slip and 3 for reverse slip) using the following expression (partially adapted from Boore and Atkinson [44]):

$$\ln(SDR) = c_1(\mathbf{M} - 6.6) + c_2 SS + c_3 NS + c_4 RS + c_5\left(\sqrt{R_{rup}^2 + h^2} - 1\right) + c_6\left(\ln\left(\sqrt{R_{rup}^2 + h^2} - 1\right)\right) + c_7 \ln(V_{s30}/760) \quad (1)$$

where SDR is the geometric mean of the two SDRs obtained for the two perpendicular components of the ground motion and c_{1-7} and h are the coefficients that are to be found through regression analysis. …. The regression was performed using the two-step regression procedure of Joyner and Boore [45], [46], which provides for an event-specific mean misfit, which is similar to an event term in a GMM developed using mixed effects regression. The mean misfit in this case is referred to as the between-event SDR residual, δW_{SDR}. Note that δW_{SDR} is an event property, and as such represents the average misfit of the recordings from that event (used for the present analyses) relative to the model in Equation 1. Figure 3-2 shows the predicted maximum SDR values from Equation 1 for the 2- and 20-story buildings as a function of distance for three magnitudes. The predicted values are for a strike slip fault and $V_{s30} = 760\ m/s$.

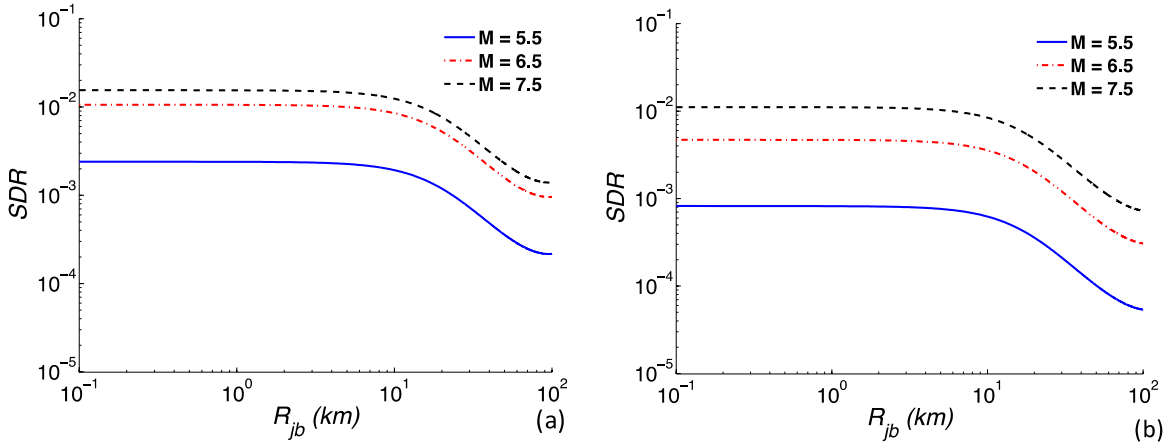

Figure 3-2. Trends between maximum SDR and distance for three different magnitudes and a) 2-story and b) 20-story buildings

Table 3-2 summarizes coefficients c_{1-7} and h obtained through regression analysis on the SDR prediction equation presented in Equation 1. Figure 3-3 shows the intra- and inter-event residuals for the 2- and 20-story buildings obtained in the first and second stages of the two-step regression analysis described in Section 3.2.

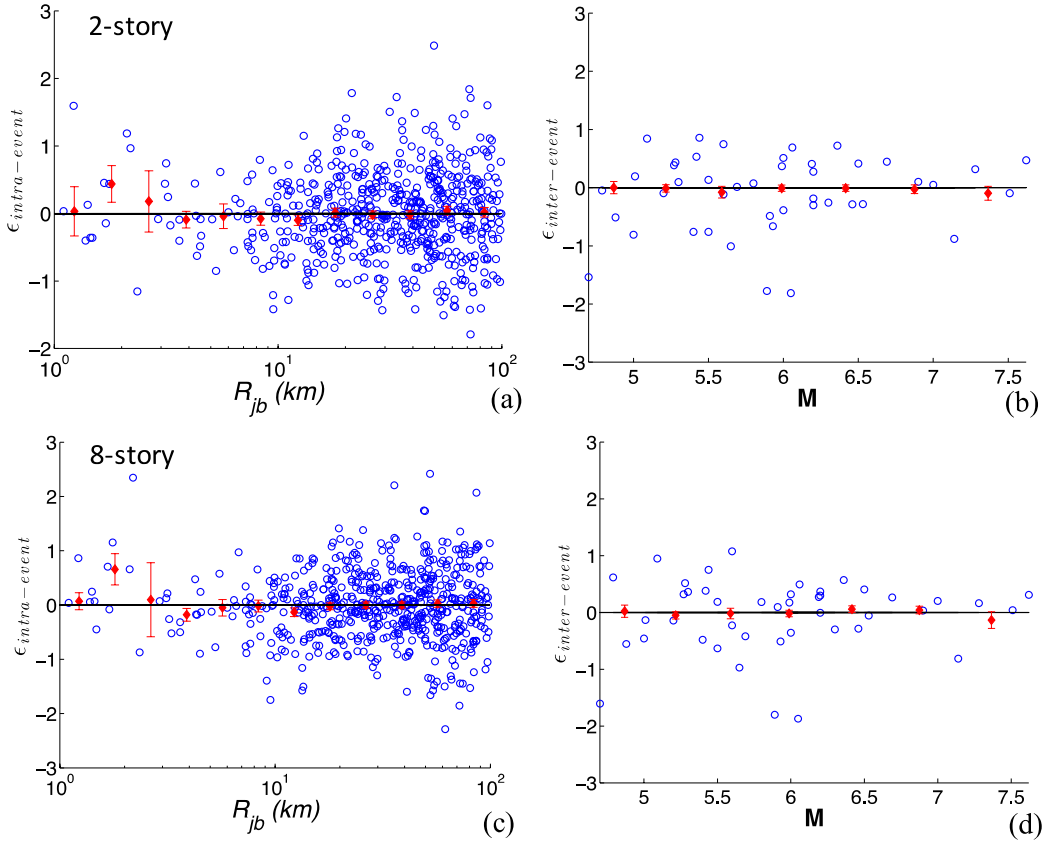

Figure 3-3. Intra and inter-event residuals obtained from the two-stage regression analysis on the 2- and 20-story buildings

Table 3-2 Regression coefficients of Equation 1

Building	c_1		c_2	c_3	c_4	c_5	c_6	c_7	h
	$\mathbf{M} \leq 6.6$	$\mathbf{M} > 6.6$							
2-Story	1.486	0.255	5.990	5.484	5.695	0.037	24.211	-3.574	-0.617
4-Story	1.596	0.510	-0.637	-1.093	-1.078	0.007	12.416	-1.543	-0.775
8-Story	1.563	0.585	-3.459	-3.810	-3.964	-0.009	4.355	-0.693	-0.963
12-Story	1.640	0.699	-1.685	-2.096	-2.154	0.003	10.548	-1.392	-1.018
20-Story	1.743	0.762	2.918	2.481	2.467	0.026	20.120	-2.915	-1.005

We investigate correlation between EDPs produced by mainshock vs aftershock ground motions by computing correlation coefficients between δW_{SDR} terms for parent mainshocks and

their respective children aftershocks. Results of these analyses are provided in Table 3-3, which indicates correlation coefficients between 0.10 and 0.35 for the various structural models. To provide a baseline against which these correlations can be compared, we use the second set of 474 mainshock δW_{SDR} terms from 17 events as follows: (1) calculate δW_{SDR} from mainshocks; (2) split the set of 17 events into six parent and eleven children events; (3) each parent event will be assigned two children events; and (4) calculate the correlation coefficient of the paired values from Step 3. The resulting correlation coefficients, shown on the right side of Table 3-3, range from 0.0-0.20 and are always lower than those for the properly paired MS-AS events. The large differences observed in the two sets of correlation coefficients indicate that correlation of parent-to-child event ground motions is an important factor at the EDP level. This suggests that DS-MS-AS and TG-MS-MS pairings, which would not be expected to preserve this correlation structure, may be problematic. This is explored further below.

Table 3-3. Correlation coefficients between actual and randomly-assigned 'parent' and mean 'children' SDR event terms

Building	Correlation coefficient between SDR event terms	
	Actual	Randomly-assigned
2-story	0.07	0.10 (0.0)
4-story	0.24	0.26 (0.10)
8-story	0.31	0.35 (0.19)
12-story	0.24	0.25 (0.1)
20-story	0.14	0.15 (0.02)

3.3 Collapse performance assessment

3.3.1 Methodology

Buildings that have been subjected to a mainshock event and sustained structural damage are usually not repaired during the short period immediately following the mainshock when the rate of aftershocks is highest. This, coupled with the accumulation of structural damage under successive aftershock events, results in a significant uncertainty regarding the state of a structure when subsequent aftershocks occur. The Markov process [47, 48] accounts for this uncertainty in the state of the structure. Each element P_{ij} of the Markov transition matrix in Equation 2 is the

probability of transitioning from damage state i when the building is subjected to a seismic event to damage state j under the successive earthquake.

$$\Pi = \begin{bmatrix} P_{11} & P_{12} & \cdots & P_{1r} \\ 0 & P_{22} & \cdots & P_{2r} \\ \vdots & \vdots & \ddots & \vdots \\ 0 & 0 & \cdots & P_{rr} \end{bmatrix} \quad (2)$$

Damage states become incrementally more severe as the index of the transition probabilities increases. The Markov transition matrix in Equation 2 is of the upper triangular form as no repair measure is assumed to take place to restore the building to a less severe damage state during the time the building is subjected to aftershocks. The last element in each row in Equation 2 represents the probability of the most extreme limit state, which herein is defined as collapse. Each element P_{ij} in Equation 2 can be obtained through Equation 3.

$$P_{ij} = \int \left(P_{i,j}^{DS}\left[EDP > edp_j | IM\right] - P_{i,j+1}^{DS}\left[EDP > edp_{j+1} | IM\right]\right) d\lambda_{IM}(im) \quad (3)$$

In Equation 3, the integrand is the probability of the structure being in damage state j given that it has already experienced damage state i when subjected to the previous event. λ_{IM} is the mean rate of exceedance of the intensity measure (IM) that links the response of the building to the seismic hazard at the building's location and can be obtained through aftershock probabilistic seismic hazard analysis (APSHA) [9]. The rate of aftershocks decays with the time following the mainshock [21]. APSHA utilizes a nonhomogeneous recurrence Poisson process with a rate that accounts for the temporal decay in the rate of aftershocks in lieu of a time-independent recurrence assumption made by the conventional PSHA [9]. The time-variant rate of aftershocks implies that, in the aftershock environment, the P_{ij} term in Equation 3 will be a function of the elapsed time since the mainshock's occurrence. Consequently, the Markov transition matrix in Equation 2 is also time-dependent.

An implicit assumption in Equation 3 is that, during the time window for which the performance is being evaluated, the likelihood of more than one event triggering the damage state transition is negligible. Therefore, use of Equation 3 in the post-mainshock environment requires discretization of time into sufficiently short intervals such that no more than one aftershock is likely within each interval. At time step m following the mainshock, the probability

that the structure is in damage state j given that damage state i has already occurred under the mainshock is equal to the element on row i and column j of matrix P^m in Equation 4.

$$P^m = \prod_{i=1}^{m} \Pi^i \tag{4}$$

Evaluation of seismic performance without conditioning on the occurrence of a mainshock (i.e, in the pre-mainshock environment) must account for uncertainties in the occurrence of the mainshock as well as the state of the structure following the mainshock. This can be done by multiplying the limit state transition matrix in Equation 4 by a vector of P_i^{MS} values as illustrated in Equation 5. The vector of P_i^{MS} values represents the probability of the structure being in damage state $i, i = 1, \dots, r$ under mainshock ground motions. The elements of the vector P_i^{MS} can be calculated by integrating building fragility curves obtained by subjecting the building to mainshock ground motions ($P_{MS}^{DS}[EDP > edp_i|IM] - P_{MS}^{DS}[EDP > edp_{i+1}|IM]$ in Equation 6) together with the seismic hazard curve obtained through mainshock PSHA (λ_{IM} in Equation 6).

$$P^m = (P_1^{MS}, \dots P_r^{MS}) \prod_{i=1}^{m} \Pi^{\mathrm{i}} \tag{5}$$

$$P_i^{MS} = \int (P_{MS}^{DS}[EDP > edp_i|IM] - P_{MS}^{DS}[EDP > edp_{i+1}|IM]) d\lambda_{IM}(im) \tag{6}$$

Figure 3-4 presents the mainshock and aftershock seismic hazard curves developed for a hypothetical point site located within 10 km of a 5-km-long line fault with a rate of 0.1 events per year [49]. The aftershock hazard curves are calculated using the APSHA methodology formulated by Yeo and Cornell [9] while the mainshock hazard curves are obtained through conventional PSHA [50]. The APSHA hazard curves are calculated for a time window of one year following the mainshock. The IM utilized for the hazard analyses is the spectral acceleration at the first mode period of the structure being examined $\left(S_a(T_1)\right)$. The parameters that define the spatial distribution of the earthquake magnitudes as well as the temporal decline in the rate of aftershocks are adopted from generic California model by Reasenberg and Jones [51]. The largest aftershock is assumed to be identical to its causative mainshock in magnitude. A magnitude range of 5 to 7 is assumed for the mainshocks. The minimum magnitude is taken as 5 since events with smaller magnitudes are not likely to induce notable damage in code-conforming structures.

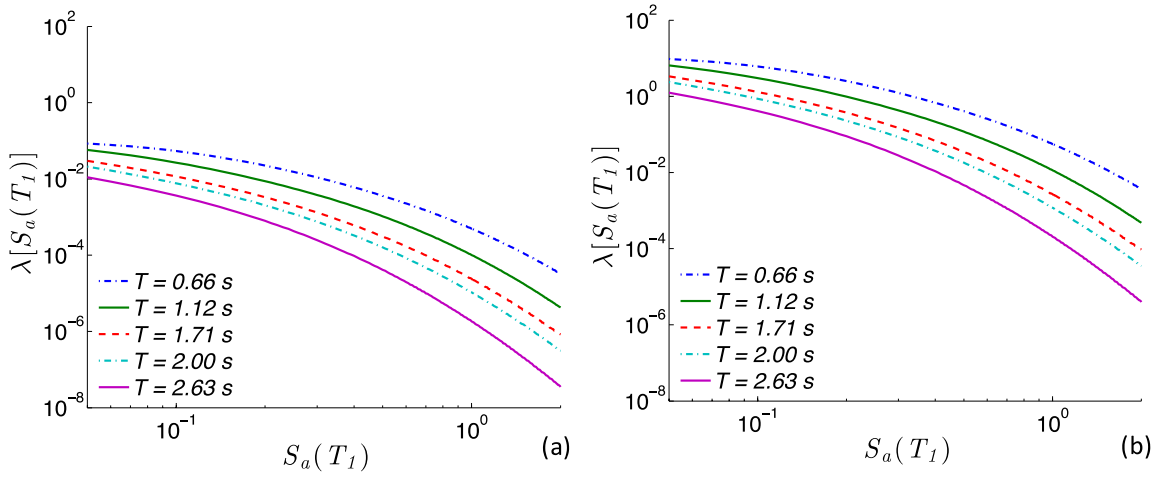

Figure 3-4. (a) Mainshock and b) Aftershock hazard curves for the five studied structures

To obtain collapse fragility curves for the five buildings, we begin by performing nonlinear response history analyses on the structural models using the first ground motion in each record-pair. The goal of this step is to induce a certain level of SDR in the structure. Four incrementally-increasing damage states, as well as the intact state under the first ground motion in each pair, are targeted. These states range from intact to 5% maximum story drift ratio (SDR_{GM1}). The five SDR_{GM1} values serve as proxies for the possible states of structural and non-structural damage under a mainshock ground motion. Table 3-4 summarizes examples of structural and non-structural damage states associated with each of the SDR_{GM1} values. These four levels of SDR values together with the intact state also serve as the possible damage states that the building could be in under each of the ground motions in a cluster of seismic events before collapse occurs. In other words, they are necessary for populating the elements of the Markov transition matrix in Equation 2. Collapse state is defined as the point of dynamic instability.

P_{MS}^{DS} values required as input to Equation 6 are obtained by fitting a lognormal fragility curve to each of the five damage states [52]. Next, we perform nonlinear response history analysis using the second ground motion in the record-pairs, to obtain the post-mainshock capacity of the damaged building for each of the maximum SDR_{GM1} values from the previous step. The second-event ground motions are scaled to twelve different $S_a(T_1)$ levels. These S_a values, together with the maximum SDR values obtained by subjecting the building to the scaled aftershocks, are used to estimate the fragility curves needed to compute the $P_{i,j}^{DS}[EDP > edp_j|IM]$ in Equation 3 using the method described in Baker [53].

Table 3-4. Limit state description

SDR	Damage state description[1]
1%	Severe cracking in partition walls, cracking in floor slabs
2%	Minor damage in beams and columns
2.75%	Concrete cracking and spalling in beams and columns
5%	Significant concrete spalling, fracture or buckling in longitudinal reinforcement, punching shear failure in slabs

[1]From Haselton et al. [54] and FEMA P-58 [5]

3.3.2 Outcomes of nonlinear dynamic analyses under the sets of sequential ground motions

In this section we compare the outputs of nonlinear dynamic analyses performed on the five structures subjected to the four sets of mainshock-aftershock records shown in Table 2-1. Our objectives are to examine the impact of correlation between parent and children event on seismic performance as well as to evaluate whether appropriately selected mainshock records can be used as the second ground motion in a sequence. Following the TG-MS-MS protocols, such record pairs can be selected to maintain the appropriate magnitude and distance relationship between the first and second ground motion (details in Table 2-1). SS-MS-AS record pairs comprise actual mainshock-aftershock ground motion sequences and serve as the benchmark against which other options are compared. The outcomes of the nonlinear dynamic analyses under the four ground motions are contrasted in two different contexts. First, we compare the drift profiles of each building obtained by subjecting it to the second-event ground motions in the four record-pair sets. Variations in drift profile along the height are a function of both the dynamic properties of the structure as well as the frequency content of the ground motion being examined. As such, differences in the drift profiles under the second event ground motions will reflect the differences in the frequency content of mainshock and aftershock ground motions.

Most structures that conform to modern seismic design guidelines can withstand a major seismic event without experiencing extensive structural damage that would lead to collapse. Thus, most studies done on evaluating collapse performance of code-conforming buildings under as-recorded ground motions have used a scaled version of the strong records available in the current databases of ground motions. Later in this section, we also address how scaling the ground motions in the four record-pair sets and the subsequent changes in their frequency content would impact the outcomes of collapse performance assessment.

Figure 3-5 compares the median drift profiles obtained by subjecting each of the five studied buildings to the unscaled second event ground motions in the four record-pair sets described in Section 2.2. For all buildings, the second event ground motions of the MS-MS set induce higher displacement demands compared to the other three record sets. The 2-story building experiences significantly higher drift demands when subjected to the MS-MS set. This is not surprising given that the dominant spectral content of the MS-MS ground motions corresponds to periods closer to the first mode period of the 2-story building when compared to the remaining three sets (Figure 2-3). In general, the median drift profiles under the SS-MS-AS, DS-MS-AS and TG-MS-MS sets are not notably different. This observation is somewhat expected given the proximity of the dominant frequency contents of the second event ground motions in these three record sets at periods close to the first mode of dynamic response or higher modes (which become more influential in the taller buildings). The amplification of higher modes of response under the stronger content of the MS-MS set at periods close to those of the higher modes of response (Table 3-1) can be observed in the median drift profiles of the taller buildings shown in Figure 3-5c-e. In the 8- 12- and 20-story buildings, where the presence of higher modes is more significant, the SDR at the higher stories where higher modes are more influential is higher when the buildings are subjected to the second ground motions in the MS-MS set.

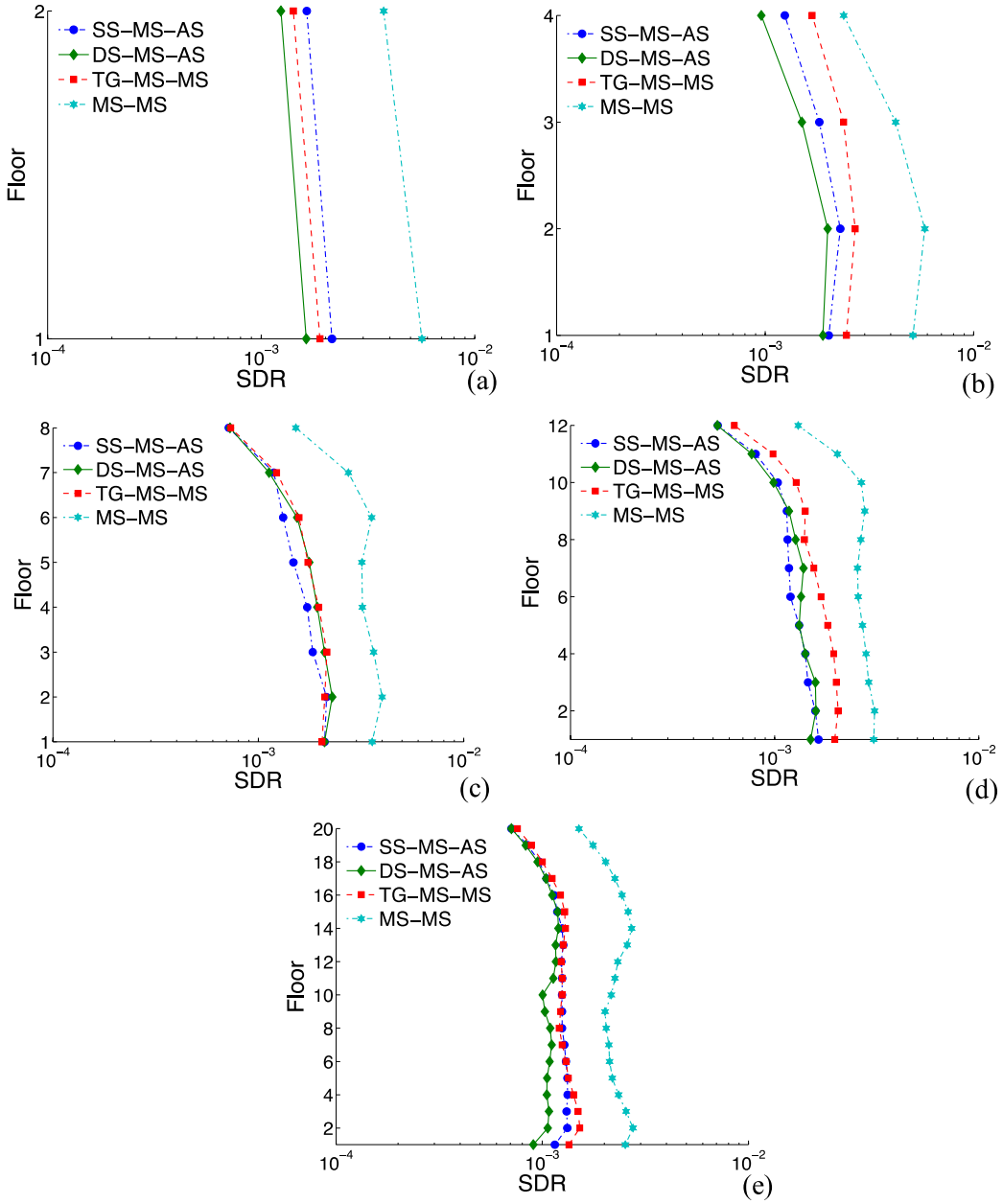

Figure 3-5. Comparing median drift profiles under the unscaled second event ground motions in the four record-pair sets for the five studied buildings

The focus of the rest of the current section is placed on comparing the collapse performance of the five RC frame buildings under the four record-pair sets. Figure 3-6 shows the collapse fragility curves for the 4- and 20-story structures using the SS-MS-AS ground motions. As described in Section 3.3.1, these fragilities are based on scaling of the aftershock ground motions until a collapse state is achieved in the numerical model. The 'intact' results in Figure 3-6 represent a condition of no damage from the mainshock (all damage results from aftershocks). The other results in Figure 3-6 represent varying levels of mainshock-damaged states as

represented by SDR_{GM1} values ranging from 1-5%. Median collapse capacities ($\hat{S}a_{col}$) for the intact structures are 0.70g and 0.40g for the 4- and 20-story buildings, respectively. As expected, performance worsens ($\hat{S}a_{col}$ decreases) as SDR_{GM1} increases. These reductions are appreciable (factors of 2 to 4) for the most severe damage state, ($SDR_{GM1} = 5\%$).

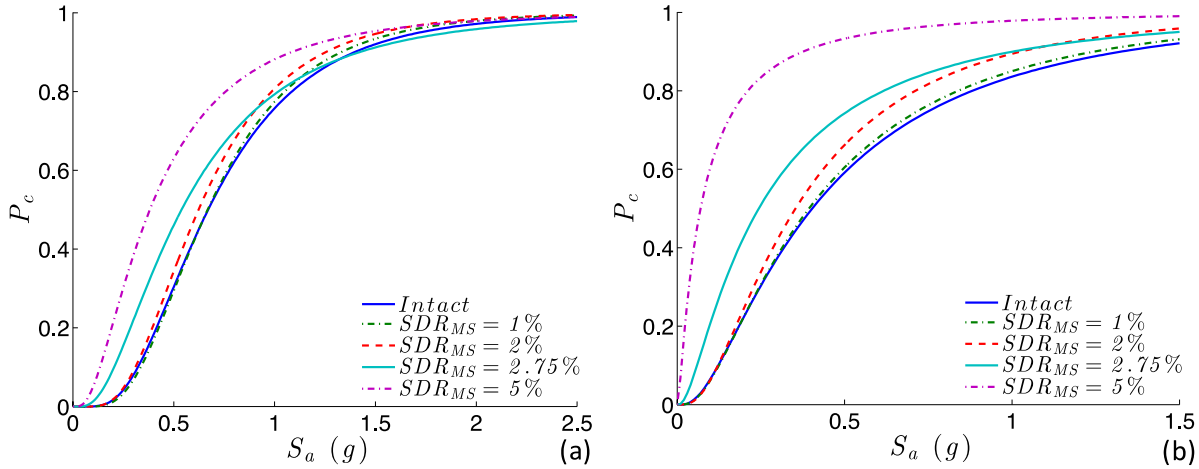

Figure 3-6. Collapse fragility curves for the intact and incrementally-increasing mainshock-damaged states for the (a) 4- and (b) 20-story structures under the SS-MS-AS set

Figure 3-7 compares the collapse fragility curves for the 2- and 20-story structures under all four ground motion sets. In both buildings, collapse is more likely when response history analyses are done using the ground motions in the SS-MS-AS set whereas the MS-MS set results in the lowest collapse likelihoods. This observation might seem counterintuitive at first glance given the stronger spectral content of the MS-MS set in Figure 2-3b and the higher displacement demand that the second event ground motions in the MS-MS set found to be likely to induce in the studied buildings. However, the trends seen in Figure 3-7 can be better explained when the impact of the scaling scheme used in collapse analysis on the spectral content of the ground motions is considered. We will further discuss the impact of scaling the ground motions on the outcomes of nonlinear dynamic analyses when we compare life service collapse risk under the four record-pair sets.

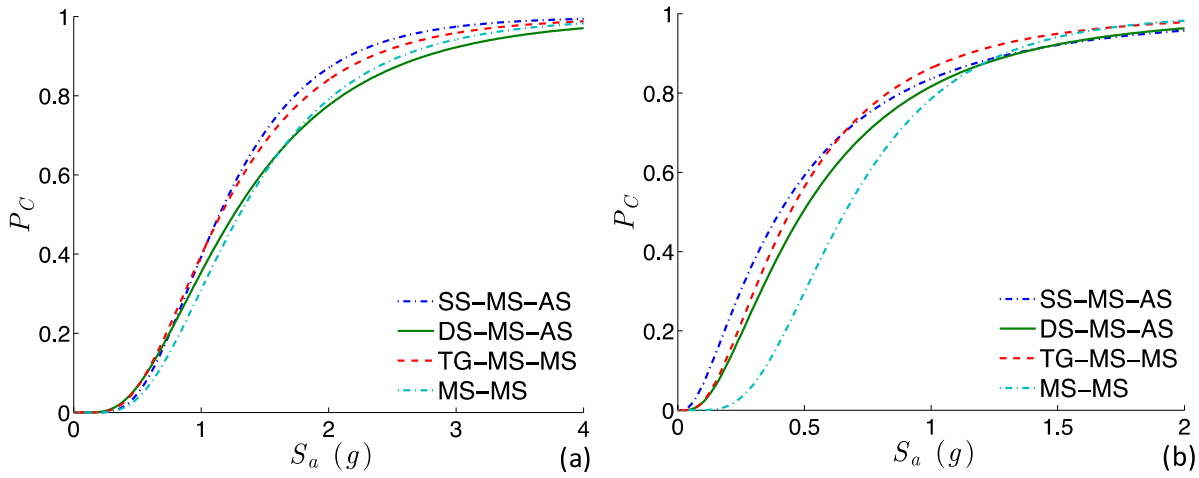

Figure 3-7. Collapse fragility curves of (a) 2- and (b) 20-story structures under the four record-pair sets in the intact state after the first event ground motions

We next turn to the question of collapse probabilities derived by convolving the fragility curves from Figure 3-6 with hazard curves for the example hypothetical site (Figure 3-4). We use an assumed lifespan of 50 years for the five buildings, with the results in Figure 3-9, Figure 3-10 and Figure 3-11. The collapse probability at each time step is obtained using the Poisson distribution in Equation 7, where the rate of the collapse limit state (λ_c) is obtained through Equation 5. An underlying assumption in Equation 7 is that the building will be restored to its pre-damaged state after an event sequence (mainshock and the following aftershocks). In other words, while the state of the building under successive aftershocks is modeled probabilistically, its state before the occurrence of the next cluster of mainshock and aftershock events is modeled deterministically. Based on this assumption, the probability of collapse is computed as:

$$P_c = 1 - e^{-\lambda_c T} \tag{7}$$

Recall from Section 3.3.1 that the post-mainshock collapse capacity is obtained by first scaling the second event ground motions to twelve $S_a(T_1)$ levels and then subjecting the buildings to the scaled records. To better visualize the relative scale factors required to anchor S_a of the second event ground motions to the relevant values for the four record-pair sets across different periods, Figure 3-8a presents the ratio of the linear S_a under the SS-MS-AS set to the linear S_a values calculated under the remaining three sets of ground motions. As a measure of the relative strength of the spectral content, Figure 3-8b compares the ratio of the nonlinear pseudo acceleration (A_y) under the second event ground motion of the SS-MS-AS set to the remaining three sets for a ductility factor of 8. The relevance of the ground motion scale factors

(Figure 3-8 a) and the impact on the dominant frequency content of the ground motion (Figure 3-8b) is described in subsequent paragraphs.

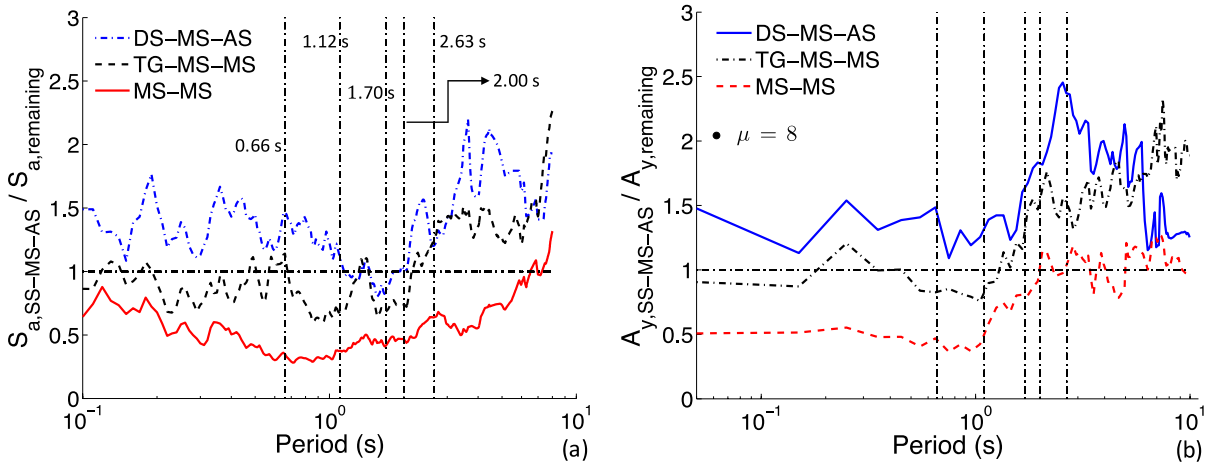

Figure 3-8. Ratio of (a) linear and (b) nonlinear spectral accelerations of the second event ground motions in the SS-MS-AS set to the remaining three sets

The collapse probability $(\hat{P}_C)$ values shown in Figure 3-9 indicate that the studied buildings are in general more likely to collapse under the SS-MS-AS set compared to the DS-MS-AS set. Figure 3-9a suggests that the DS-MS-AS set would generally require larger scale factors to be anchored to a common spectral acceleration with SS-MS-AS. Larger scale factors mean that, whereas, when scaled to a common S_a value at a target period both DS-MS-AS and SS-MS-AS would have an identical spectral value at that target period, the contents of the DS-MS-AS set is likely to be more significantly amplified at periods lower and higher than the target period. The target period is usually taken as the initial first mode period of the structure being examined. In a nonlinear structure, the role of longer periods in the dynamic response becomes more important as nonlinearities in the response shifts the period of the first mode to higher values. Depending on the dynamic characteristic of the structure, higher modes of response with periods smaller than that of the first mode could also have a significant influence on the seismic response.

The larger scale factors associated with the DS-MS-AS set at the first modes of response of the five studied buildings is mostly offset by the stronger content of the SS-MS-AS set as illustrated in Figure 3-9b. Consequently, the $\hat{P}_C$ values obtained by subjecting the buildings to the SS-MS-AS set are generally higher than those obtained under the DS-MS-AS set.

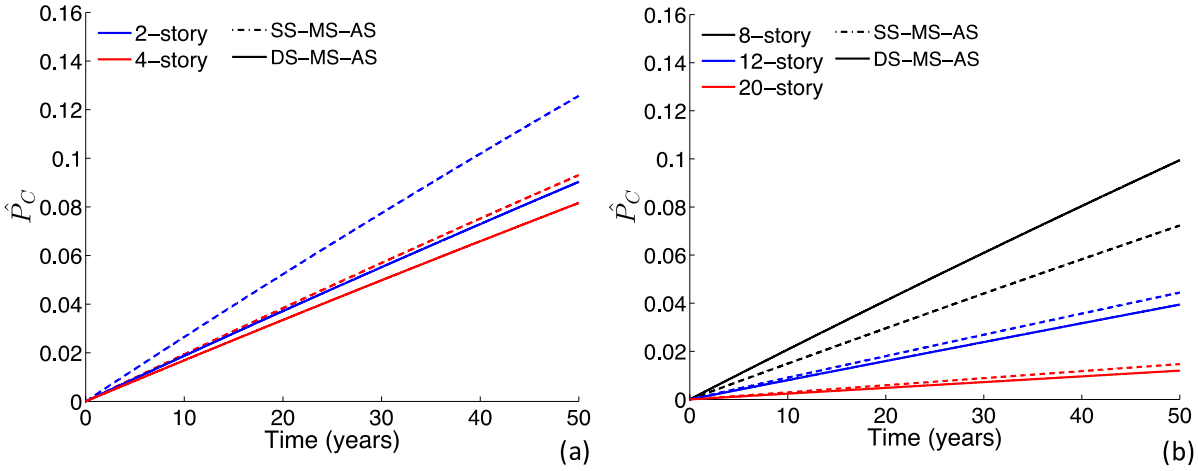

Figure 3-9. Comparing $\hat{P}_C$ for an assumed lifespan of 50 years for a) 2- and 4-story and b) 8-, 12- and 20-story buildings under the SS-MS-AS and DS-MS-AS sets of ground motions

Figure 3-10 compares $\hat{P}_C$ for the five structures subjected to the SS-MS-AS and TG-MS-MS record sets. For the 2-story building (Figure 3-10a), the two record-pair sets yield almost identical $\hat{P}_C$ values. This result can be understood by the similarities in both the ratio of linear spectral values at the first mode period of the 2-story building in Figure 3-8a as well as the nonlinear response spectra for the SS-MS-AS and TG-MS-MS record sets for periods < ~2 seconds (Figure 2-3). Recall from Table 3-1 that the first mode period of the intact 2-story structure is 0.66 seconds, which even after lengthening is unlikely to exceed the range where the nonlinear spectra significantly differ. The 4-story building (initial T_1 = 1.12 sec) would be expected to have a dynamic response at the collapse level that is controlled by portions of the nonlinear spectra where the SS-MS-AS set is stronger than the TG-MS-MS set. The stronger content of the SS-MS-AS set is further amplified by the higher scale factor required to anchor its linear S_a at $T = 1.12s$ to an identical value with TG-MS-MS set ($S_a(T = 1.12s)$ is smaller for the SS-MS-AS set in Figure 3-8a). Consequently, as shown in Figure 3-10a, the collapse risk will be higher in the 4-story building when collapse analysis is done using the record-pairs of the SS-MS-AS set.

Figure 3-10b shows that the trends between $\hat{P}_C$ obtained under the SS-MS-AS and TG-MS-MS sets for the 8- and 12-story buildings follow a similar trend to what observed before for the 4-story building. The observed trends for the 8- and 12-story buildings can be explained in the similar background as that used to compare $\hat{P}_C$ under the SS-MS-AS and TG-MS-MS sets for the 4-story building. The $\hat{P}_C$ values obtained by subjecting the 20-story building to the record-pairs

in the SS-MS-AS and TG-MS-MS are less different. The SS-MS-AS nonlinear spectrum is stronger at periods closer to the initial and elongated first mode periods of the 20-story building. However, a larger scale factor is associated with the TG-MS-MS set in Figure 3-8a at $T_1 = 2.63s$. This, together with a combination of a more significant presence of higher modes in the dynamic response of the 20-story building and the proximity of the contents of the ground motions in the two record sets at short periods close to those of the higher modes (Figure 3-8b) results in closer $\hat{P}_C$ under the SS-MS-AS and TG-MS-MS sets in the 20-story building.

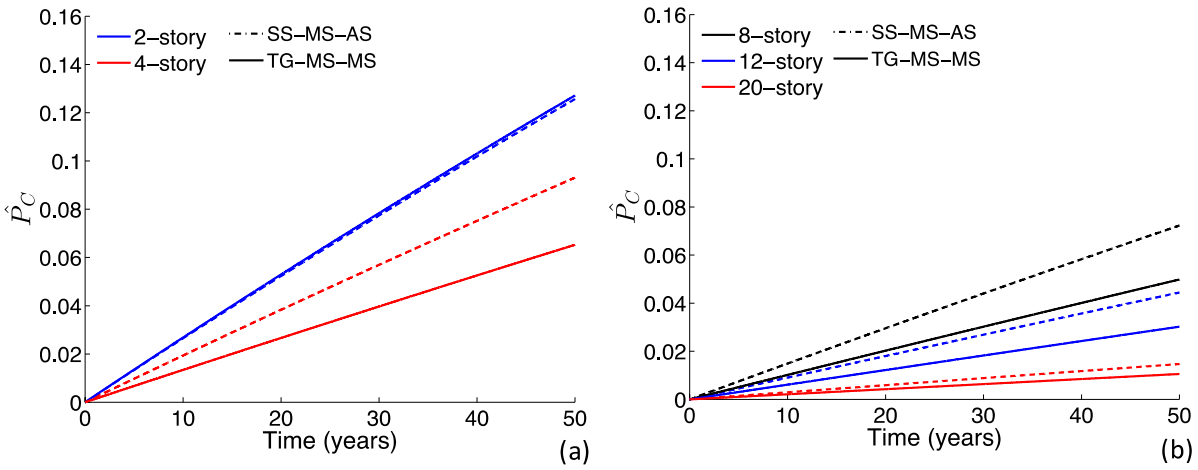

Figure 3-10. Comparing $\widehat{P}_C$ for an assumed lifespan of 50 years for a) 2- and 4-story and b) 8-, 12- and 20-story buildings under the SS-MS-AS and TG-MS-MS sets of ground motions

The $\hat{P}_C$ values obtained from the SS-MS-AS and MS-MS record sets are compared in Figure 3-11. Over the 50 years of service life, collapse is more likely when the buildings are subjected to the SS-MS-AS set as compared to MS-MS. At first glance, this is in contradiction with the trends in Figure 2-3b where the nonlinear spectral values of the MS-MS are higher than or in the proximity of those associated with the SS-MS-AS. However, Figure 3-8a suggests that the factors required to scale the spectral accelerations of both sets to a common value are much larger for the SS-MS-AS set compared to the MS-MS set. Given that, as period increases, the nonlinear response spectra of both sets (Figure 3-8b) start to converge faster compared to the linear response spectra used to compute the scale factors (Figure 3-8a), a higher scale factor for the SS-MS-AS records means that the scaled second event ground motions in this set will be stronger than those in the scaled MS-MS set. The difference between $\hat{P}_C$ under the two sets is more significant in the 4-story building where its relatively low initial first mode period results in a much larger scale factor under the SS-MS-AS set whereas its elongated first mode period

would place it in a point where the nonlinear scaled contents of the SS-MS-AS set are likely to far exceed those of the MS-MS set. The $\hat{P}_C$ plots under the two sets are less notably different for the 2-story building where its low first mode period means that, despite having larger scale factors for the SS-MS-AS ground motions, its dynamic response is mostly influenced by the contents with frequencies where the MS-MS set is notably stronger than the SS-MS-AS set. The $\hat{P}_C$ values show less variation between the SS-MS-AS and MS-MS sets in Figure 3-11b for the 8-, 12- and 20-story structures. This is not surprising given the closer scale factors for both sets at higher periods associated with first mode periods of these buildings and the more significant presence of higher modes with lower periods in the dynamic response of the taller buildings where the energy content of the MS-MS set is stronger than the SS-MS-AS set.

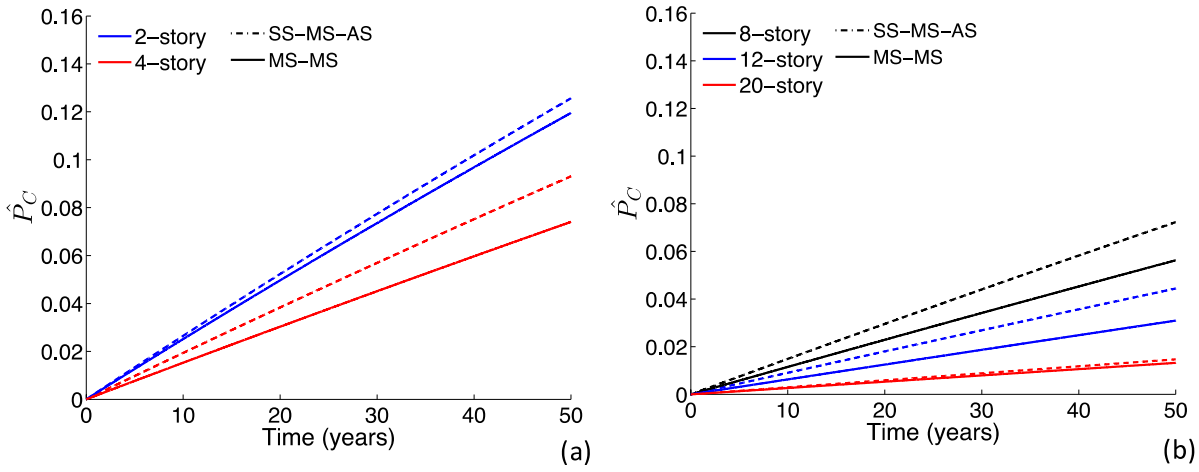

Figure 3-11. Comparing $\widehat{\boldsymbol{P}}_{\boldsymbol{C}}$ for an assumed lifespan of 50 years for a) 2- and 4-story and b) 8-, 12- and 20-story buildings under the SS-MS-AS and MS-MS sets of ground motions

4 SUMMARY AND CONCLUSION

A key to obtaining realistic assessments of the seismic performance of structures from nonlinear dynamic analysis is the proper selection of the ground motions. The selected records must, as much as possible, reflect the ground motions that the structure is most likely to experience during its service life. In the absence of systematic guidelines for selecting record-pairs for seismic performance assessment under sequential ground motions, using mainshock ground motions as both records in ground motion pairs has become a common practice. However, evidence from past studies on the differences in the frequency content of mainshock and aftershock ground motions casts doubt on the accuracy of such practice. In this study, we investigate the impact of two main issues related to mainshock-aftershock record selection: (1) how the frequency contents of mainshock and aftershock events differ, and (2) the presence of correlation in parent mainshock to child aftershock ground motions. The impact of both of these issues on displacement demand and collapse probabilities are illustrated for structures having a range of heights (2 to 20 stories).

Notable differences in the frequency content of mainshock and aftershock ground motions are observed when the inelastic response spectra of 100 records are compared. The mainshock ground motions are found to contain richer frequency content at lower periods while the aftershock records show higher spectral values at higher periods. Such observations are consistent with predictions of some prior ground motion models. These differences in frequency content produce notable differences in displacement demand and collapse capacities obtained from a benchmark mainshock-aftershock record set and three sets of record-pairs complied using alternative approaches. The difference in the dynamic response of the studied buildings was found to be influenced primarily by the frequency content differences between the record-pair sets near the first mode period of the structural models, and to a lesser extent by frequency content differences near higher mode frequencies.

Past studies have reported a mild correlation between the event terms of the ground motions recorded from parent and children event. We demonstrate this effect as strongly present in the displacement-based EDP of maximum SDR. The strong difference observed in the SDR event terms from randomly-assigned and actual parent and children events indicates that the SS-MS-AS record-pair selection approach is preferable to the DS-MS-AS approach.

Based on the findings presented here, we recommend that the current practice of using pairs of mainshock-mainshock ground motions for nonlinear dynamic analysis be discontinued. We recommend use of SS-MS-AS record sets, which places a premium on documentation of aftershock ground motions following major events as ground motion databases continue to expand and develop.

REFERENCES

1. Burton, H.V., et al., Framework for incorporating probabilistic building performance in the assessment of community seismic resilience. *Journal of Structural Engineering*, 2015: p. C4015007.
2. Kazama, M. and T. Noda, Damage statistics (Summary of the 2011 off the Pacific Coast of Tohoku Earthquake damage). *Soils and Foundations*, 2012. **52**(5): p. 780-792.
3. Stewart, J.P. and G. Lanzo. *2016 CENTRAL ITALY EARTHQUAKE SEQUENCE*. 2016; Available from: http://www.geerassociation.org/index.php/component/geer_reports/?view=geerreports&id=76.
4. Atzori, S., et al., The 2010–2011 Canterbury, New Zealand, seismic sequence: multiple source analysis from InSAR data and modeling. *Journal of Geophysical Research: Solid Earth*, 2012. **117**(B8).
5. Federal Emergency Management Agency (FEMA), *FEMA P-58: Seismic performance assessment of buildings*. 2012: Redwood City, CA.
6. Wooddell, K.E. and N.A. Abrahamson, Classification of main shocks and aftershocks in the NGA-West2 database. *Earthquake Spectra*, 2014. **30**(3): p. 1257-1267.
7. Boyd, O.S., Including foreshocks and aftershocks in time-independent probabilistic seismic-hazard analyses. *Bulletin of the Seismological Society of America*, 2012. **102**(3): p. 909-917.
8. Iervolino, I., M. Giorgio, and B. Polidoro, Sequence-based probabilistic seismic hazard analysis. *Bulletin of the Seismological Society of America*, 2014. **104**(2): p. 1006-1012.
9. Yeo, G.L. and C.A. Cornell, A probabilistic framework for quantification of aftershock ground-motion hazard in California: Methodology and parametric study. *Earthquake Engineering & Structural Dynamics*, 2009. **38**(1): p. 45-60.
10. Hatzigeorgiou, G.D. and D.E. Beskos, Inelastic displacement ratios for SDOF structures subjected to repeated earthquakes. *Engineering Structures*, 2009. **31**(11): p. 2744-2755.
11. Nazari, N., J. van de Lindt, and Y. Li, Effect of mainshock-aftershock sequences on woodframe building damage fragilities. *Journal of Performance of Constructed Facilities*, 2013. **29**(1): p. 04014036.
12. Raghunandan, M., A.B. Liel, and N. Luco, Aftershock collapse vulnerability assessment of reinforced concrete frame structures. *Earthquake Engineering & Structural Dynamics*, 2015. **44**(3): p. 419-439.
13. Ryu, H., et al. *Developing fragilities for mainshock-damaged structures through incremental dynamic analysis*. in *Ninth Pacific Conference on Earthquake Engineering, Auckland, New Zealand*. 2011.
14. Jeon, J.S., et al., Framework of aftershock fragility assessment–case studies: older California reinforced concrete building frames. *Earthquake Engineering & Structural Dynamics*, 2015. **44**(15): p. 2617-2636.
15. Burton, H.V. and M. Sharma, Quantifying the Reduction in Collapse Safety of Mainshock-Damaged Reinforced Concrete Frames with Infills. *Earthquake Spectra*, 2016.
16. Goda, K., Nonlinear response potential of mainshock–aftershock sequences from Japanese earthquakes. *Bulletin of the Seismological Society of America*, 2012. **102**(5): p. 2139-2156.

17. Ruiz-García, J., Mainshock-aftershock ground motion features and their influence in building's seismic response. *Journal of Earthquake Engineering*, 2012. **16**(5): p. 719-737.
18. Ruiz-García, J. and J.C. Negrete-Manriquez, Evaluation of drift demands in existing steel frames under as-recorded far-field and near-fault mainshock–aftershock seismic sequences. *Engineering Structures*, 2011. **33**(2): p. 621-634.
19. Shcherbakov, R. and D.L. Turcotte, A modified form of Båth's law. *Bulletin of the Seismological Society of America*, 2004. **94**(5): p. 1968-1975.
20. Boore, D.M., et al., NGA-West2 equations for predicting PGA, PGV, and 5% damped PSA for shallow crustal earthquakes. *Earthquake Spectra*, 2014. **30**(3): p. 1057-1085.
21. Utsu, T. and Y. Ogata, The centenary of the Omori formula for a decay law of aftershock activity. *Journal of Physics of the Earth*, 1995. **43**(1): p. 1-33.
22. Goda, K., Record selection for aftershock incremental dynamic analysis. *Earthquake Engineering & Structural Dynamics*, 2015. **44**(7): p. 1157-1162.
23. Baker, J.W. and C. Allin Cornell, Spectral shape, epsilon and record selection. *Earthquake Engineering & Structural Dynamics*, 2006. **35**(9): p. 1077-1095.
24. Bradley, B.A., et al., Prediction of spatially distributed seismic demands in specific structures: Ground motion and structural response. *Earthquake Engineering & Structural Dynamics*, 2010. **39**(5): p. 501-520.
25. Luco, N. and C.A. Cornell, Structure-specific scalar intensity measures for near-source and ordinary earthquake ground motions. *Earthquake Spectra*, 2007. **23**(2): p. 357-392.
26. Boore, D.M. and G.M. Atkinson, Spectral scaling of the 1985 to 1988 Nahanni, Northwest Territories, earthquakes. *Bulletin of the Seismological Society of America*, 1989. **79**(6): p. 1736-1761.
27. Chiou, B., et al., NGA project strong-motion database. *Earthquake Spectra*, 2008. **24**(1): p. 23-44.
28. Abrahamson, N., W. Silva, and R. Kamai, *Update of the AS08 Ground-Motion Prediction equations based on the NGA-west2 data set*. 2013, Pacific Earthquake Engineering Research Center, College of Engineering, University of California, Berkeley.
29. Chiou, B.-J. and R.R. Youngs, An NGA model for the average horizontal component of peak ground motion and response spectra. *Earthquake Spectra*, 2008. **24**(1): p. 173-215.
30. Kagan, Y.Y., Aftershock zone scaling. *Bulletin of the Seismological Society of America*, 2002. **92**(2): p. 641-655.
31. Massey Jr, F.J., The Kolmogorov-Smirnov test for goodness of fit. *Journal of the American statistical Association*, 1951. **46**(253): p. 68-78.
32. Ruiz-García, J. and E. Miranda, Inelastic displacement ratios for evaluation of existing structures. *Earthquake Engineering & Structural Dynamics*, 2003. **32**(8): p. 1237-1258.
33. Miranda, E., Inelastic displacement ratios for structures on firm sites. *Journal of Structural Engineering*, 2000. **126**(10): p. 1150-1159.
34. Veletsos, A., N. Newmark, and C. Chelapati. *Deformation spectra for elastic and elastoplastic systems subjected to ground shock and earthquake motions*. in *Proceedings of the 3rd world conference on earthquake engineering*. 1965.
35. Chopra, A.K. and C. Chintanapakdee, Inelastic deformation ratios for design and evaluation of structures: single-degree-of-freedom bilinear systems. *Journal of structural engineering*, 2004. **130**(9): p. 1309-1319.

36. Tothong, P. and C.A. Cornell, An empirical ground-motion attenuation relation for inelastic spectral displacement. *Bulletin of the Seismological Society of America*, 2006. **96**(6): p. 2146-2164.
37. Chopra, A.K., *Dynamics of structures*. Vol. 3. 1995: Prentice Hall New Jersey.
38. Haselton, C.B., *Assessing Seismic Collapse Safety of Modern Reinforced Concrete Moment Frame Buildings*, in *PhD Dissertation*. 2007, Department of Civil and Environmental Engineering, Stanford University.
39. American Society of Civil Engineers (ASCE), *ASCE/SEI 7-05: Minimum design loads for buildings and other structures*. 2005: Reston, VA.
40. American Concrete Institue (ACI), *ACI 318M-02: Building code requirements for structural concrete and commentary*. 2002: Farmington Hills, MI.
41. Mazzoni, S., et al., *OpenSees command language manual*. 2006, Pacific Earthquake Engineering Research Center, University of California, Berkeley.
42. Ibarra, L.F., R.A. Medina, and H. Krawinkler, Hysteretic models that incorporate strength and stiffness deterioration. *Earthquake engineering & structural dynamics*, 2005. **34**(12): p. 1489-1511.
43. Haselton, C.B., et al., Seismic collapse safety of reinforced concrete buildings. I: Assessment of ductile moment frames. *Journal of Structural Engineering*, 2010. **137**(4): p. 481-491.
44. Boore, D.M. and G.M. Atkinson, Ground-motion prediction equations for the average horizontal component of PGA, PGV, and 5%-damped PSA at spectral periods between 0.01 s and 10.0 s. *Earthquake Spectra*, 2008. **24**(1): p. 99-138.
45. Joyner, W.B. and D.M. Boore, Methods for regression analysis of strong-motion data. *Bulletin of the Seismological Society of America*, 1993. **83**(2): p. 469-487.
46. Joyner, W.B. and D.M. Boore, Methods for regression analysis of strong-motion data. *Bulletin of the Seismological Society of America*, 1994. **84**(3): p. 955-956.
47. Iervolino, I., M. Giorgio, and E. Chioccarelli, Markovian modeling of seismic damage accumulation. *Earthquake Engineering & Structural Dynamics*, 2015.
48. Yeo, G.L. and C.A. Cornell, *Stochastic characterization and decision bases under time-dependent aftershock risk in performance-based earthquake engineering*. 2005, Pacific Earthquake Engineering Research Center, College of Engineering, University of California, Berkeley.
49. Baker, J.W., *An introduction to probabilistic seismic hazard analysis*, in *Report for the US Nuclear Regulatory Commission, page Version*. 2008.
50. Kramer, S.L., *Geotechnical earthquake engineering*. 1996: Pearson Education India.
51. Reasenberg, P.A. and L.M. Jones, Earthquake hazard after a mainshock in California. *Science*, 1989. **243**(4895): p. 1173-1176.
52. Yeo, G.L. and C.A. Cornell, *Stochastic characterization and decision bases under time-dependent aftershock risk in performance-based earthquake engineering*. 2005: Pacific Earthquake Engineering Research Center.
53. Baker, J.W., Efficient analytical fragility function fitting using dynamic structural analysis. *Earthquake Spectra*, 2015. **31**(1): p. 579-599.
54. Haselton, C., et al., *An Assessment to Benchmark the Seismic Performance of a Code-Conforming Reinforced concrete Moment-Frame Building, PEER 2007/12*. 2007, Berkeley, CA: Pacific Earthquake Engineering Research Center, University of California, Berkeley.